

Towards integrated data analysis of divertor diagnostics with ray-tracing

M. Carr¹, A. Meakins¹, A. Baciero², M. Bernert³, A. Callarelli¹, A. Field¹, C. Giroud¹, J. Harrison¹, N. Hawkes¹, S. Henderson⁴, B. Lipschultz⁵, T. Lunt³, D. Moulton¹, F. Reimold⁶, ASDEX Upgrade Team, JET contributors[†], MAST-Upgrade team and the EUROfusion MST1 Team[‡]

¹ CCFE, Culham Science Centre, Abingdon, Oxon, OX14 3DB, UK.

² Laboratorio Nacional de Fusión, CIEMAT, Madrid, Spain

³ Max-Planck-Institut für Plasmaphysik, 85748 Garching, Germany.

⁴ Department of Physics SUPA, University of Strathclyde, Glasgow, G4 0NG, UK.

⁵ York Plasma Institute, Department of Physics, University of York, Heslington, York, UK.

⁶ Forschungszentrum Jülich GmbH, Institut für Energie-und Klimaforschung-Plasmaphysik, 52425 Jülich, Germany

1. Introduction

Building a better understanding of divertor physics for ITER and DEMO will require developing techniques that can integrate information from multiple diagnostics into a unified analysis of the underlying plasma properties. The charge-exchange recombination and beam analysis (CHERAB) code was developed at JET as a platform for modelling spectroscopic diagnostics with the Raysect ray-tracing package¹. The framework is capable of handling detailed 3D engineering geometry and spectrally resolved metallic reflections. In this work CHERAB has been extended for use with filtered imaging and bolometry, two diagnostics that can particularly benefit from the ray-tracing approach.

2. Lighting equations, materials and Monte-Carlo integration

The total visible radiation power measured by a detector is given by the integral of the incident radiance over the collecting solid angle Ω and surface area A .

$$I = \int_A \int_{\Omega} L_i(p, \omega_i) \times \cos(\theta_i) d\omega_i dA$$

Here, $L_i(p, \omega_i)$ is the incident radiance at a given point p and incident angle ω_i on the observing surface. Similarly, the amount of light reflected by a surface is given by the integral of all incoming radiance over 2π steradians multiplied by the bidirectional reflectance distribution function (BRDF). The BRDF is a weighting function that describes the redistribution of incident light into outgoing reflections and transmission/absorption. It is commonly approximated in terms of two ideal material components, specular and diffuse reflections. Real physical materials exhibit more complex behaviours. For this work, the BRDFs of fusion relevant materials were modelled with the Cook-Torrance BRDF^{4,5}.

The lighting integrals were evaluated using Monte-Carlo integration, which approximates the integral with a weighted average^{2,6}. The lighting integrals can be naturally discretised in terms of N sample points on pixel area A and N sample vectors over the hemisphere Ω . To optimise the convergence rate of integration, importance sampling was used⁶.

[†] Litaudon et al, "Overview of the JET results in support to ITER", accepted for publication in Nuclear Fusion

[‡] Meyer et al, "Overview of progress in European Medium Sized Tokamaks towards an integrated plasma-edge/wall solution", accepted for publication in Nuclear Fusion.

4. Bolometry

Bolometry is a diagnostic particularly sensitive to the machine geometry due to the effect of volume sampling. Sightlines from the ASDEX Upgrade (AUG) bolometer foils were ray-traced with a path tracing algorithm. For every detector surface a bundle of rays are traced through the instrument and machine geometry while sampling the radiance along their ray paths. By using the full 3D machine model, effects such as occlusion and vignetting were included in the étendue calculations.

Fig. 1 compares the response matrix on a course tomography grid for a single detector generated with the single ray line-of-sight approximation (LOS) and light cone methods. The LOS method leads to higher spatial frequencies in the response function, due to aliasing effects on a course grid. Fig. 2 compares the sight line densities for the whole AUG foil bolometer detector set calculated with the two methods. For the LOS technique there are many cells in the plasma that are effectively dark, i.e. not seen by any detector. While in the LOS approach, emission from this region would be neglected, the volume sampled calculation shows that they are also contributing to the measured signal. This can lead to a misinterpretation of the radiated power profile, especially in the case of very localised radiation.

Fig. 3 shows the relative error in the calculated detector power between the two techniques. The calculation used an example emission profile from AUG shot 33280 at 4.1s. For many detectors the LOS technique is a good approximation. However, the errors can become significant ($> 10\%$) for sightlines that see emission regions with strong gradients, such as the x-point radiation. This could have implications for determination of the total radiated power, although it is not possible to draw general conclusions since the errors will very much depend on the emission scenario.

5. JET calibration photos

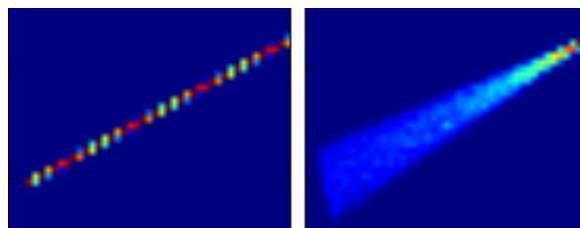


Figure 1: Comparison of sensitivity matrices in the poloidal plane for a bolometer foil modelled with a single sight line and a volume sampled light cone.

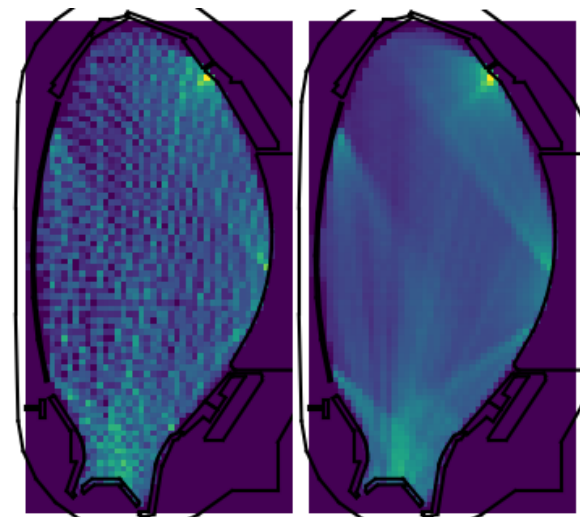


Figure 2: Comparison of the sight line densities for foil bolometers at AUG modelled with single ray paths and volume sampled light cones.

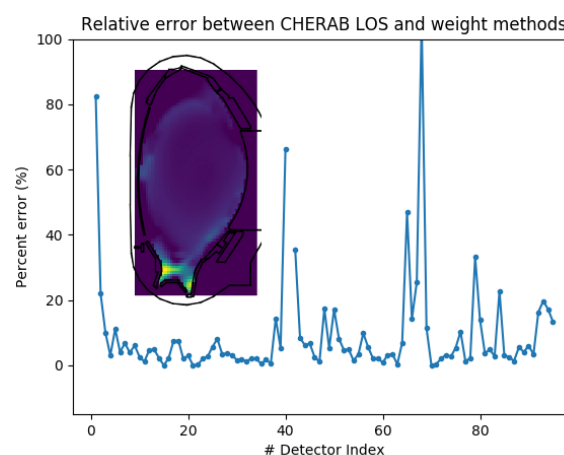


Figure 3: Percentage error in the calculated detector power when using the single ray approximation for an example AUG radiation scenario (inlet).

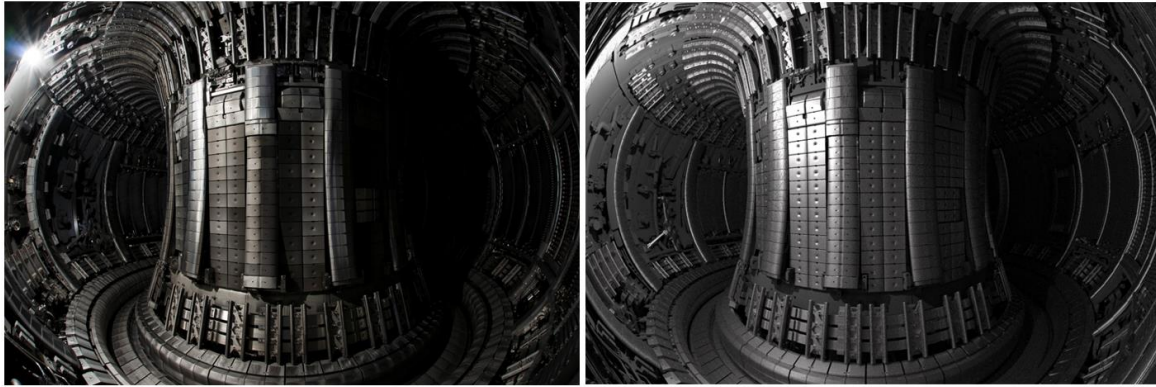


Figure 4: Measured (left) and simulated (right) image of JET in-vessel light source for calibration and benchmarking of material BRDF properties.

The material reflection model was benchmarked with calibration photos of a point light source at JET. The calibration images were rendered with a computer aided design (CAD) 3D model of the JET first wall, split into material groups. Good qualitative agreement was achieved, see Fig. 4 for an example calibration image and the companion simulation image.

The Cook-Torrance material BRDFs were implemented with refractive index data for bulk Be and W^{7,8}. The surface roughness parameter was approximated by eye. The regions of greatest disagreement in Fig. 4 tend to be in the coated CFC tile groups. These materials have non-trivial surface properties. In future work, the tile BRDF model could be improved by fitting the refractive index and roughness parameters with measured tile data.

6. Filtered camera images

SOLPS simulations were used as inputs to an emission model for representative plasma scenarios in AUG and MAST-U, see figure 5. In the MAST-U image the edge emission of the plasma is predicted to be much less pronounced than in MAST due to the closed divertor design which increases the neutral gas compression ratio between the mid-plane and divertor. Fig 5b shows a filtered Da camera simulation for AUG diagnostic camera 06Bul03.

Inverting these images with a directly ray-traced forward model would be infeasible due to the immense computational resources required for reflection ray-tracing. However, let us make the assumption that the camera viewing geometry and the machine first wall conditions are not changing significantly between shots. This means that the only thing changing during a shot is the distribution of emitters. The reflection properties and their

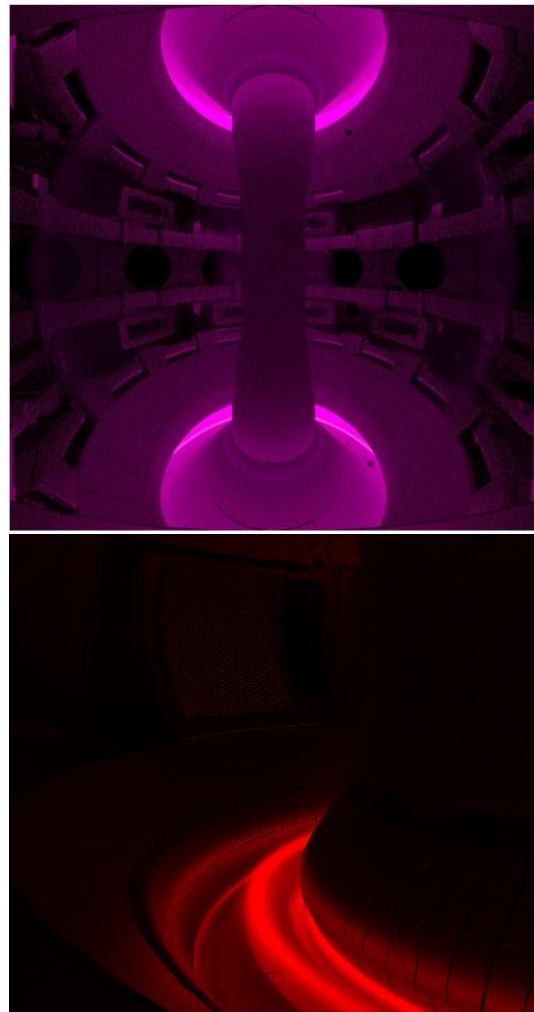


Figure 5: (Top) Simulated image of visible emission from the Balmer series in MAST-U as would be measured by the mid-plane camera. (Bottom) Simulated filtered Da image for AUG camera 06Bul03

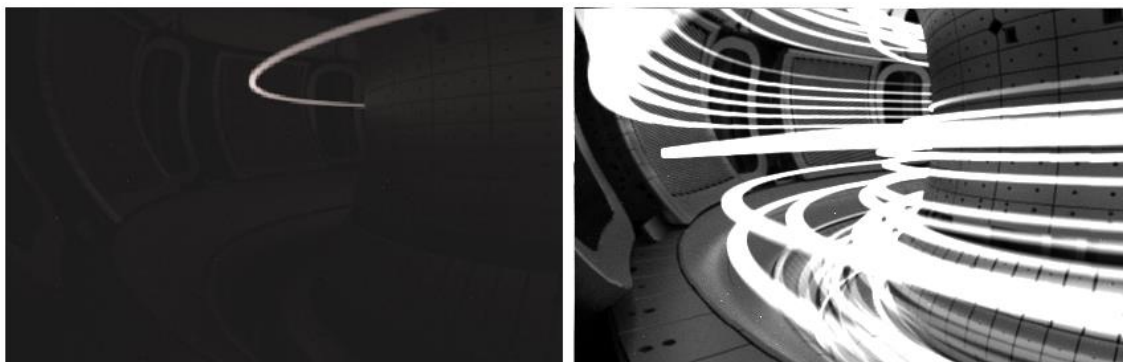


Figure 6: (Left) A slice of the reflections matrix representing a single Green's function. (Right) Forward image produced by matrix multiplication of a random set of Green's functions.

responses to individual geometric sources are a constant. Therefore, we can use the ray-tracing technique to generate a set of Green's functions that describe the coupling of individual emitting plasma sources into the observer equation. Fig. 6a shows an individual Green's function for a discrete toroidally symmetric plasma source. A measured camera image can be de-constructed into a linear combination of the underlying source Green's functions. Fig. 6b shows a forward image created by matrix multiplication with a random set of source functions.

The resulting sensitivity matrix allowed camera inversions to be performed with established tomography techniques. Although each individual ray-traced image can take several hours to compute, a typical inversion with the SART algorithm⁸ and cached reflection matrix was performed in under 5mins on a standard desktop I7 PC without any further ray-tracing.

Conclusions

Volume sensitivity matrices of AUG foil bolometers were calculated with ray-tracing including geometry effects such as occlusion and vignetting. The relative errors between the single ray and ray-bundle methods were shown to be significant for a sample AUG radiation scenario. Filtered divertor imaging was modelled with physically realistic reflections using a Cook-Torrance BRDF model for W and Be. To allow reflection effects to be included in inversions, a set of Green's functions were developed for the underlying SOLPS emission sources. Subsequent camera inversions were performed without on-demand raytracing.

Acknowledgements

This work has been carried out within the framework of the EUROfusion Consortium and has received funding from the Euratom research and training programme 2014-2018 under grant agreement No 633053. The views and opinions expressed herein do not necessarily reflect those of the European Commission.

References

- ¹ Raysect – www.raysect.org
- ² Pharr, M. & Humphreys, G. (2016). *Physically based rendering: From theory to implementation*. Morgan Kaufmann.
- ³ Montes, R. & Urena, C. (2012). *An overview of BRDF models*. University of Grenada, Technical Report LSI-2012-001.
- ⁴ Cook, R.L. and Torrance, K.E., (1982). *A reflectance model for computer graphics*. ACM Transactions on Graphics (TOG), 1(1), pp.7-24.
- ⁵ Veach, E., (1997). *Robust Monte Carlo methods for lighting simulation*. PhD thesis, Stanford University.
- ⁶ Rakic, A.D. et al. (1998). *Optical properties of metallic films for vertical-cavity optoelectronic devices*. Applied optics, 37(22), pp.5271-5283.
- ⁷ Refractive index database - www.refractiveindex.info
- ⁸ Gordon, R. et al. (1970). *Algebraic reconstruction techniques (ART) for three-dimensional electron microscopy and X-ray photography*. Journal of theoretical Biology, 29(3), pp.471-481.